PROFILED LEADING EDGE GROOVE TILTING PAD JOURNAL BEARING FOR LIGHT LOAD OPERATION

by

Stephen L. Edney

Rotordynamics Group Supervisor

John K. Waite

Analytical Engineer, Rotordynamics

Dresser-Rand Company

Steam Turbine Division

Wellsville, New York

and

Scan M. DeCamillo

Research Manager

Kingsbury, Inc.

Philadelphia, Pennsylvania

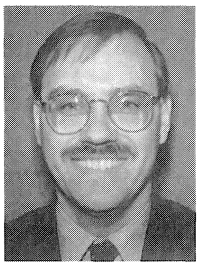

Stephen L. Edney is Supervisor of the Rotordynamics Group at the Steam Turbine Division of Dresser-Rand in Wellsville, New York. In this capacity, he is responsible for providing all of the division's technical support on rotor and bearing dynamics. These duties cover prediction of rotordynamics performance, troubleshooting field vibration problems, and conducting research programs.

Prior to joining Dresser-Rand, Dr. Edney held two positions at GEC-Alsthom in the UK. He spent six years at the Engineering Research Centre in the Tribology Group, followed by two years at Ruston Gas Turbines Limited, Aero Engine and Technology Division. While at Ruston Gas Turbines, he spent one year at GE Aircraft Engines, Cincinnati, Ohio, on a technology exchange program.

Dr. Edney received his B.Sc. (1983) and Ph.D. (1990) degrees (Mechanical Engineering) from the University of Nottingham, England. He is a member of ASME and the Vibration Institute, and a graduate member of the IMechE. He has authored, or coauthored, six technical papers.

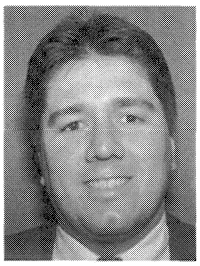

John K. Waite is an Analytical Engineer in the Rotordynamics Group of the Steam Turbine Division of Dresser-Rand in Wellsville, New York.

Mr. Waite graduated from the State University of New York at Buffalo with a B.S. (1988) degree (Mechanical Engineering). He has worked at his current position since 1990. His primary responsibilities include complete lateral and torsional rotordynamic analysis on production steam turbines and driven equipment. Other responsibilities include bearing analysis, field vibration analysis, and bearing case support stiffness testing. Prior to joining Dresser-Rand, Mr. Waite worked for two years as a Design Engineer with McGard, Inc. in Buffalo, New York.

Mr. Waite is a member of ASME and the Vibration Institute.

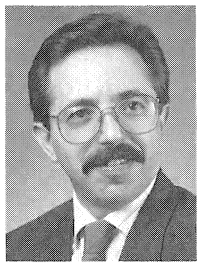

Scan M. DeCamillo is Research Manager for Kingsbury, Inc. He is responsible for design, tests, analysis, and development of Kingsbury fluid film bearings for worldwide industrial and military applications.

Since 1975, Mr. DeCamillo has provided engineering support to industry, being involved with selection, operation, troubleshooting and upgrading bearings in various kinds of machinery. He has developed performance and structural tools for bearing analysis, established design criteria for bearings in nuclear, naval, and power applications, and has contributed bearing data and criteria to ASM, AISE, EPRI, and API. Current research addresses reducing power loss and temperature in high speed, pivoted shoe bearings.

Mr. DeCamillo received his B.S. degree (Mechanical Engineering) from Drexel University. He is a registered Professional Engineer in the State of Pennsylvania and a member of ASME, STLE, ASM, and the Vibration Institute.

ABSTRACT

Optimization of a leading edge groove tilting pad journal bearing for application in a small, high speed, multistage steam turbine is described. Rotordynamics constraints to meet a design objective maximum operating speed of 18000 rpm resulted in a rotor with a 51.0 in bearing span and 5.0 in diameter tilting pad journal bearings. This configuration yielded a design with projected bearing loads of less than 25 psi, and journal surface speeds that could approach 400 ft/sec. Under these conditions, the applicable limits of conventional style tilting pad journal bearings are stretched, since operation is well into the turbulent flow regime. This can result in significantly higher than predicted operating pad temperatures and increased frictional losses. Furthermore, at very light pad loads, bearing dynamic performance and influence on rotor behavior often does not correlate well with theory.

For this application, high efficiency leading edge groove bearings (journal and thrust) were used, due to their preferred steady state operating characteristics at high speed. However, as is

often observed with lightly loaded conventional style journal bearings, dynamic performance did not precisely match that predicted by theory. This was investigated by profiling the exit side of the leading edge groove with both a tapered and pocket geometry. Two case histories are presented demonstrating their effect on rotor-bearing stability and unbalance response. The modified bearings yielded greater system stability at high speeds, reduced overall vibration amplitudes, and greatly improved effective damping on passing through the rotor's first peak response speed.

INTRODUCTION

The design and optimization of the rotating element and bearings for a small, high speed, multistage steam turbine is described. The turbine application is nominally capable of producing up to 7000 hp and operating up to a maximum continuous speed of 18000 rpm. To comply with the dynamics specifications of the American Petroleum Institute (API) Standard 612 [1], the rotor design was optimized by minimizing the bearing span and overhang lengths, and increasing the shaft diameter through the journal bearings. This yielded a design with 5.0 in diameter journals that could operate at speeds of up to 400 ft/sec (at 18000 rpm) at projected pad loads of less than 25 psi. Under these conditions, bearing operation is well into the turbulent flow regime where pad temperatures and frictional losses can escalate. High pad temperatures in particular are a concern to OEMs and users of turbomachinery, since temperature limits of the babbitt material can be approached and margin against seizure reduced. Primarily for this reason, directed lubrication bearings were considered essential for this application.

Results presented herein are in two sections. The first section compares data from a comprehensive test program, assessing a leading edge groove tilting pad journal bearing with a conventional style flooded design. This evaluation addresses the steady state parameters of pad temperature and power loss, and bearing dynamic influence on rotor response. The second section discusses the application and operational performance of a leading edge groove journal bearing in several small, multistage, steam turbines. Two case histories are reviewed of a modification to the bearing that greatly improved dynamic performance in this light load application.

BEARING EVALUATION

The requirements for new bearing designs are clear: increased load carrying capacity and lower frictional losses at reduced oil flowrates, without increasing operating pad temperature. In pursuit of this, bearing manufacturers initially focused their efforts on thrust bearing design [2]. These improved designs first utilized the concept of directed lubrication technology, and have been widely used on OEM machinery over the last decade. Thrust bearings, by far, consume the most power of the total bearing system, and were the logical starting point for the development of this technology. However, it is only in recent years that this same technology has been actively applied to tilting pad journal bearings [3, 4, 5, 6]. This is because machine speeds are now nearing the limits of acceptable performance of conventional style journal bearing designs [7], particularly when service conditions require operation into the turbulent flow regime. Under these conditions, bearing losses exponentially increase, which can have a noticeable effect on a machine's overall efficiency. Likewise, increasing the oil flowrate to reduce high bearing temperatures generally only increases the size and cost of the lubrication system, and often with minimal or no effect.

Prior to the first application of a leading edge groove journal bearing in a production turbine, tests were conducted in a laboratory vehicle to compare the bearing's performance against a conventional style flooded design. The purpose of this test was twofold. First, to verify the claimed improvement in steady state (temperature and power loss) performance, and, second, to ensure of no adverse dynamic (stiffness and damping) effects on rotor behavior.

Test Vehicle

The test vehicle was a laboratory turbine capable of operating up to a maximum speed of 16500 rpm. A general arrangement of the test vehicle is shown in Figure 1. The rotor was of an integrally forged design with five wheels and a bearing span of 59.98 in, a midspan shaft diameter of 6.0 in, and 4.0 in diameter journals. The first wheel (control stage) only was bladed and steam provided the motive driving force. All other wheels were blank and were for the purpose of simulating a multistage rotor. The rotor is shown with shaft end flanges and bored overhangs that can accept different weights for the purpose of simulating overhung moments.

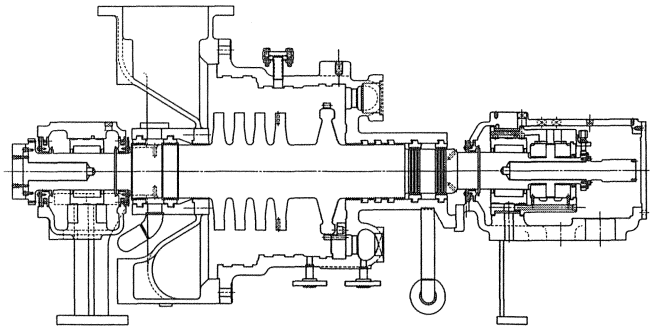

Figure 1. General Arrangement of Laboratory Steam Turbine.

Test Bearings

The test bearings were of 4.0 in diameter, 0.75 length/diameter ratio (L/D), and four pad configuration. The diametral assembled bearing clearance was nominally 1.5 mil/in of journal diameter, and loading was directed between the two lower half pads. Both bearings were designed with pad axial and circumferential alignment capability. The projected pad loads were 34.9 psi and 39.9 psi at the steam and exhaust end bearing locations, respectively. Specific features relevant to each of the test bearings are described later. Pertinent details are summarized in Table 1. Values for the assembled diametral bearing clearance were obtained by direct measurement using a precision vertical mandrel, horizontal table and dial indicator. Pad preload was based on the nominal design pad bore and measured bearing clearance. The lubricant was a light turbine oil (equivalent to ISO VG32) with a viscosity of 150 SSU at 100°F.

Table 1. Description of Laboratory Test Bearings.

BEARING TYPE	BEARING CLEARANCE mils		PAD PRELOAD		OIL FLOWRATE gpm		PIVOT OFFSET	FLOATING RING END SEALS	PAD MATERIAL
	SE	EE	SE	EE	SE	EE			
FLOODED	6.3	6.3	0.405	0.405	15.6	15.6	0.5	YES	STEEL
LEADING EDGE GROOVE	6.3	6.3	0.3	0.3	6.8	6.8	0.6	NO	STEEL

Flooded Bearing

A sectional view of the flooded design tested is shown in Figure 2. The bearing was designed with separate oil supply and oil drain orifice plugs to control flowrate. These were located in the bearing housing between each pair of neighboring pads. Oil supply was

provided by one orifice placed at the axial midposition. Oil drain was controlled via two orifices, one placed near each axial edge of the pad. Their respective locations are identified on Figure 2. Tight clearance floating ring end seals were installed at each end of the housing to ensure a flooded bearing.

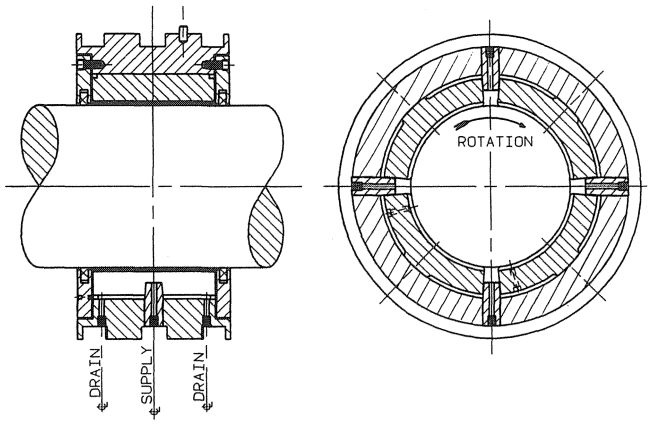

Figure 2. Conventional Style Flooded Tilting Pad Journal Bearing.

Leading Edge Groove Bearing

A sectional view of the leading edge groove design is shown in Figure 3. Oil supply to the bearing was from an annulus on the outside of the housing through a single feed tube to each pad.

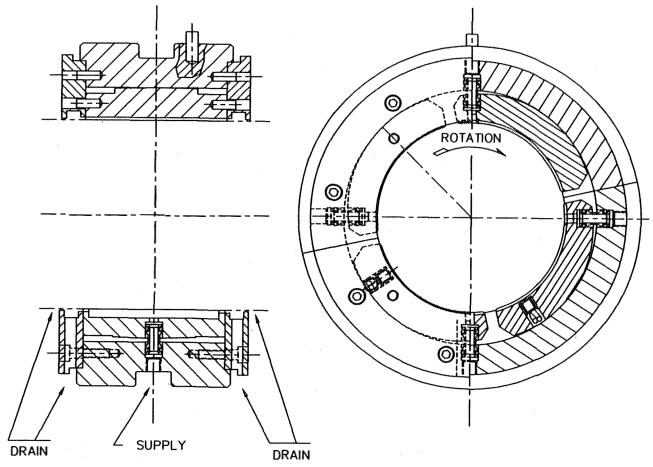

Figure 3. Leading Edge Groove Tilting Pad Journal Bearing.

These feed tubes supply cool oil directly to the center of a groove machined axially across the leading edge of each pad. This groove essentially is an extension of the pad that provides a plenum of cool oil that directly feeds the bearing. The resultant cooler oil supplied to the oil film insulates the babbitt face from hot oil carryover that adheres to the rotating journal, thus greatly reducing the babbitt temperature. Consequently, the lower pad temperatures permit lower oil flow requirements that contribute to a reduction in bearing power loss [8]. This bearing was designed with fixed open clearance end seals to allow spent hot oil to exit axially without restriction and contamination of the fresh cool supply oil. Radial drain slots located near bottom dead center also were provided in each seal.

Instrumentation

The two lower half (statically loaded) pads only were instrumented, each with a single type 'J' thermocouple temperature sensor. The sensors were located at the 75 percent position from the pad leading edge on the axial centerline, in accordance with industry standard guidelines given in API 670 [9]. This location is generally regarded as corresponding to the vicinity of the critical pad temperature. The sensors were embedded in the pads to a depth of 50 to 60 thousandths of an inch below the babbitt bond line. The babbitt material was an additional 50 to 60 thousandths of an inch thick.

Thermocouple temperature sensors also were used to measure the oil supply and oil drain temperatures. Turbine type flowmeters were used to measure the oil flowrate. The temperature rise across the bearing and the oil flowrate were used to derive a value for power loss. This was possible only on the exhaust end journal bearing. The steam end journal bearing was located in the same bearing case as the thrust, with a common oil supply and oil drain line.

Radial vibration was measured using four displacement proximity probes; two located just inboard of each journal bearing 45 degrees either side of top dead center. Shaft speed was measured from a 30 tooth wheel and displayed on a digital counter.

Test Procedure

Testing was divided into two parts separately covering an evaluation of steady state performance, and dynamic influence on rotor response.

The steady state tests were conducted over a speed range from 4000 to 16000 rpm. The turbine was assembled with the relevant test bearings. The rotor was then run up to a speed of 4000 rpm. This speed was maintained until conditions stabilized. With the oil supply temperature regulated to 120°F at a pressure of 20 psig, shaft speed was increased to 16000 rpm in increments of 1000 rpm. At each increment, two sets of readings were taken; one immediately following a speed increment, and one after pad temperature had stabilized. Data recorded were oil pressure, oil flowrate, and temperature. Temperature measurements were of the four instrumented pads, oil supply, and oil drain.

Bearing dynamic characteristics were evaluated by comparing the rotor's response to a first mode unbalance excitation. The unbalance weight used was equivalent to 4.0 oz-in placed at the rotor's midspan trim balance plane. With the weight installed, the rotor was run up to a speed of 16500 rpm and then allowed to coast down in the absence of steam forces. During coastdown, vibration data were acquired at all four radial probes over a speed range from 16000 to 500 rpm.

Test Results

Evaluation of steady state performance was in terms of pad temperature and power loss. Temperature data are given at both the steam and exhaust end bearing locations. Power loss is given at the exhaust end only and was derived from a measure of the temperature rise across the bearing and the oil flowrate. The measured pad metal temperatures are summarized in Table 2 from each test, and power loss is compared in Table 3 over a speed range of between 9000 and 16000 rpm. The following notation applies: 'SE' and 'EE' refer to the steam end and exhaust end bearing positions; and 'left' and 'right' to the thermocouple and proximity probe locations viewed from the turbine governor. When referring to thermocouple location, left is the sensor located in the downstream pad and right is the sensor located in the upstream pad.

Table 2. Summary of Measured Pad Metal Temperature.

BEARING TYPE	SE LEFT		SE RIGHT		EE LEFT		EE RIGHT	
	T_{max} °F	SPEED rpm	T_{max} °F	SPEED rpm	T_{max} °F	SPEED rpm	T_{max} °F	SPEED rpm
FLOODED	224	16000	224	15000	196	15000	234	15000
LEADING EDGE GROOVE	171	16000	186	16000	175	16000	183	16000

Table 3. Comparison of Power Loss Vs *Rotor Speed.*

BEARING TYPE	POWER LOSS (hp) @ ROTOR SPEED							
	9000 rpm	10000 rpm	11000 rpm	12000 rpm	13000 rpm	14000 rpm	15000 rpm	16000 rpm
FLOODED	8.9	10.6	12	14.6	16.9	19.4	22.1	27.5
LEADING EDGE GROOVE	8.3	10.3	11.8	13.8	15.6	17.4	18.9	20.3

Flooded Bearing

Baseline steady state data of the flooded bearings are given in Figures 4, 5, and 6. Both sets of temperature data exhibit similar trends, increasing with speed up to about 14000 rpm, where it levels off. Beyond this speed, there is some indication that the temperature may have started to decrease. At the steam end bearing, both pad temperatures agree quite closely reaching a maximum value of 224°F. At the exhaust end, some divergence in individual pad temperature is evident, with the peak reaching a value of 234°F at the pad located in the upstream position. This is contradictory to the generally accepted view that, with a load between pad arrangement, the pad located in the downstream position will indicate a higher trailing edge temperature due to mixing of hot oil carried over from the upstream pad. However, this is consistent with results from a series of tests carried out on bearings with similar pad loadings [7], and from tests with considerably higher pad loadings [10].

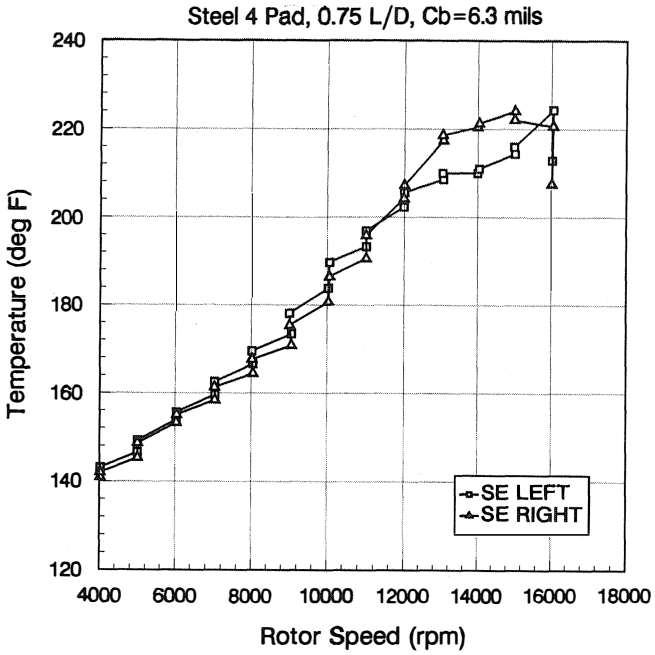

Figure 4. Steam End Pad Temperature Vs *Speed–Flooded Bearing.*

In contrast, the power consumed by the bearing continually increases with speed reaching a value of 27.5 hp at 16000 rpm. There is a clear increase in rate of power loss at around 12000 rpm. This characteristic is generally regarded as indicative of the region of transition from laminar to turbulent flow.

Vibration data are given in Figures 7 and 8 for a first mode excitation (midspan unbalance). On passing through the first critical speed, three response peaks are clearly evident at the probes located on the left side, and two response peaks at the probes located on the right side.

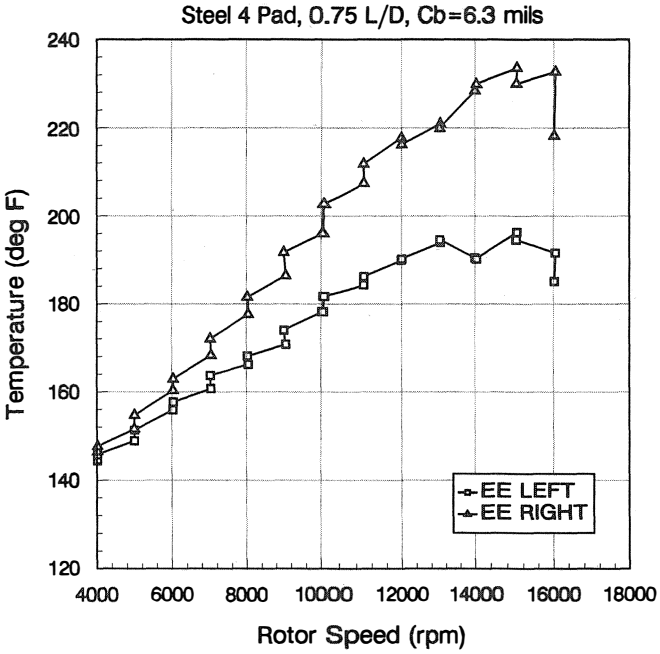

Figure 5. Exhaust End Pad Temperature Vs *Speed–Flooded Bearing.*

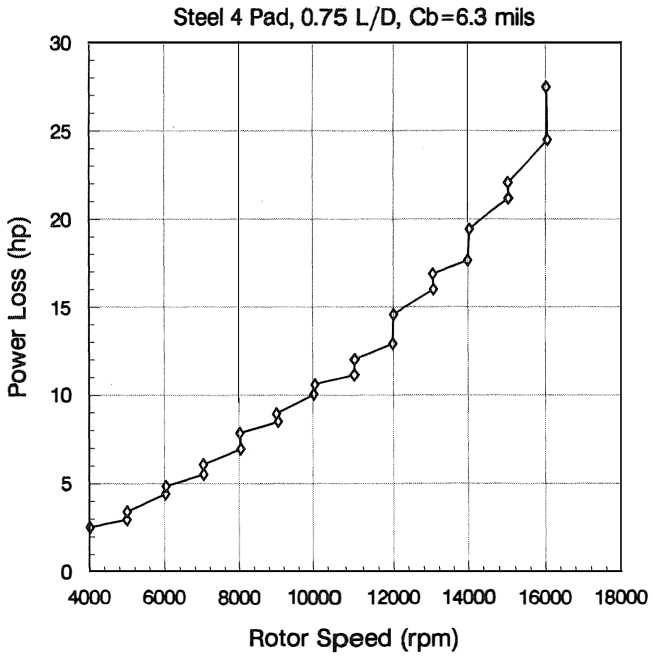

Figure 6. Exhaust End Power Loss Vs *Speed–Flooded Bearing.*

Leading Edge Groove Bearing

Steady state data of the leading edge groove bearings are given in Figures 9, 10, and 11. Clearly, the temperature data monotonically increases with speed with only a slight leveling off at around 7000 rpm. At 16000 rpm, the maximum temperature reached at both bearings is 186°F at the pad located in the upstream position. Both downstream pads indicate slightly lower pad temperatures of between 5 to 10°F. A reduction in pad temperature of some 35 to 45°F compared with the flooded design is apparent, and with 50

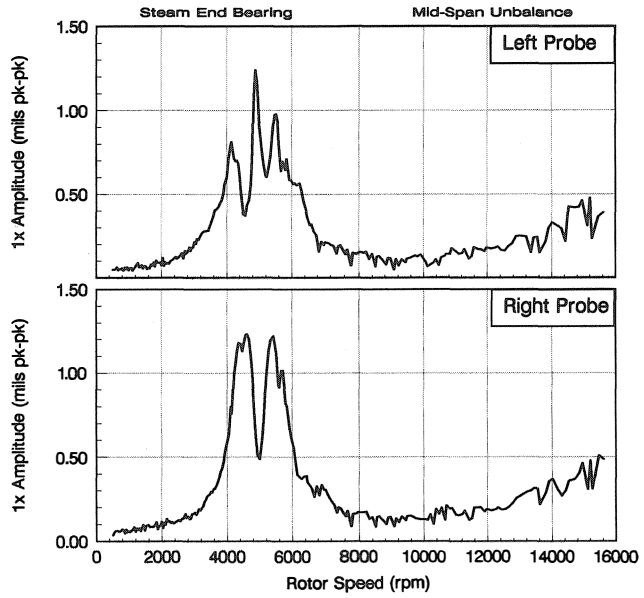

Figure 7. Measured Amplitude at Steam End Probes–Flooded Bearing.

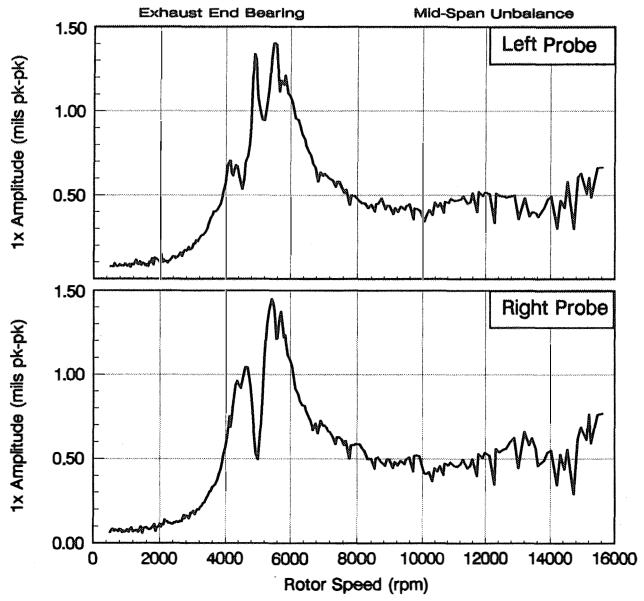

Figure 8. Measured Amplitude at Exhaust End Probes–Flooded Bearing.

percent less oil flowrate. This is partially reflected in power loss, particularly at the higher end of the speed range, which reaches a value of 20.3 hp. At 16000 rpm, this represents a reduction of approximately 25 percent compared with the flooded design.

Vibration data with the same unbalance condition are given in Figures 12 and 13. These results exhibit very similar vibration trends compared to the flooded design. The amplitude and location of discrete response peaks and troughs are near identical, as are the overall vibration levels. Clearly, the leading edge groove feature of this design has no adverse effects on bearing dynamic performance at the speed and load conditions examined.

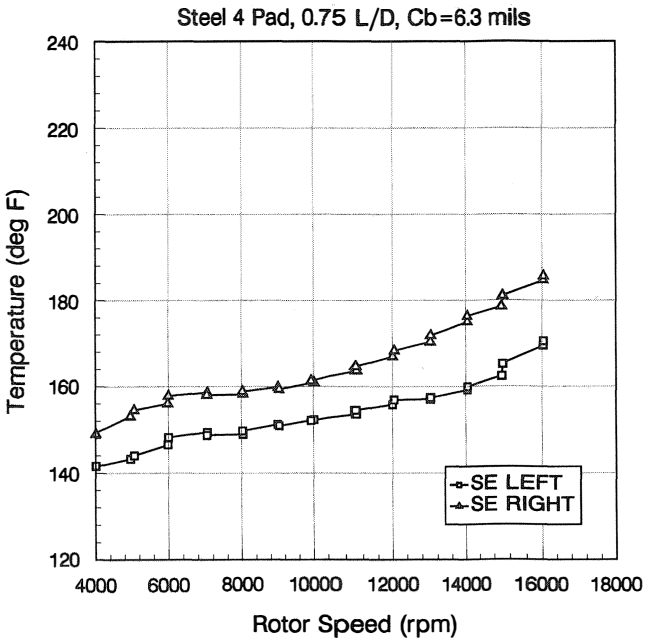

Figure 9. Steam End Pad Temperature Vs *Speed–Leading Edge Groove Bearing.*

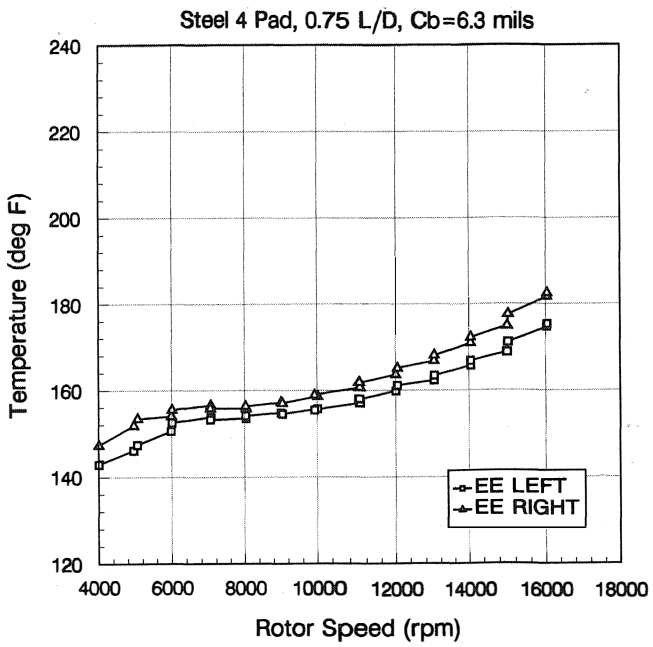

Figure 10. Exhaust End Pad Temperature Vs *Speed–Leading Edge Groove Bearing.*

BEARING APPLICATION IN A PRODUCTION TURBINE

The purpose of testing the leading edge groove bearing was for application in a small, high speed, multistage steam turbine. The turbine design is nominally capable of producing up to 7000 hp and operating up to a maximum speed of 18000 rpm. A typical configuration is illustrated in Figure 14 that is used to depict a single valve, five stage condensing design.

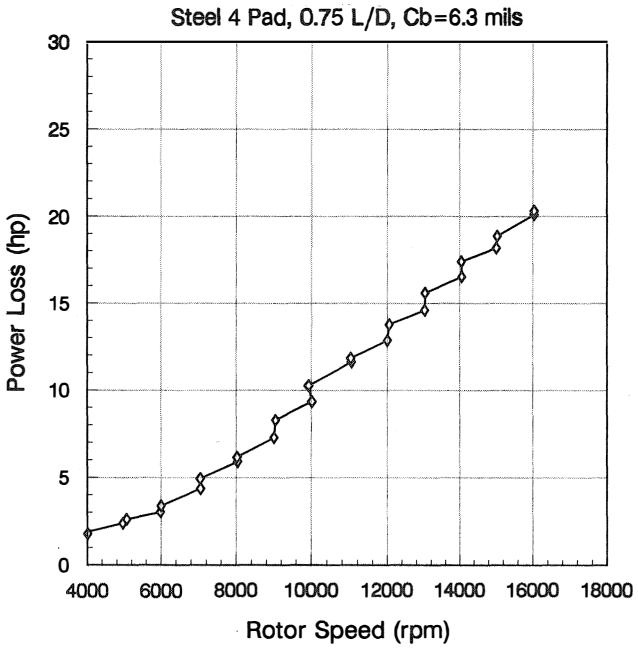

Figure 11. Exhaust End Power Loss Vs *Speed–Leading Edge Groove Bearing.*

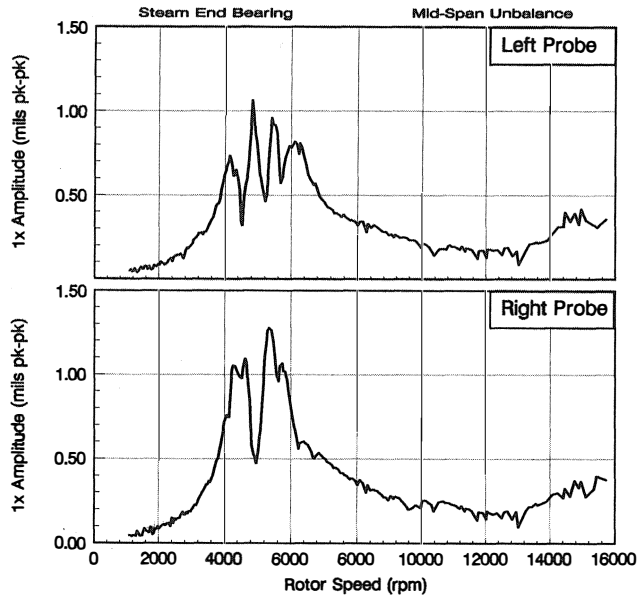

Figure 12. Measured Amplitude at Steam End Probes–Leading Edge Groove Bearing.

Rotor Design

A schematic of a typical high speed, multistage rotor is shown in Figure 15. To achieve the objective operating speed of 18000 rpm in compliance with current rotordynamics specifications [1], the bearing span and overhangs were kept to a minimum, and the shaft diameter through the journal bearings increased. This yielded a base design with a 51.0 in bearing span and 5.0 in diameter journals. The midshaft diameter was left variable in order that the rotor's dynamic characteristics could be tuned in relation to the operating speed range. For example, a five stage rotor operating at speeds approaching 18000 rpm would require a midshaft diameter of 8.5 in, to raise the location of the third lateral peak response

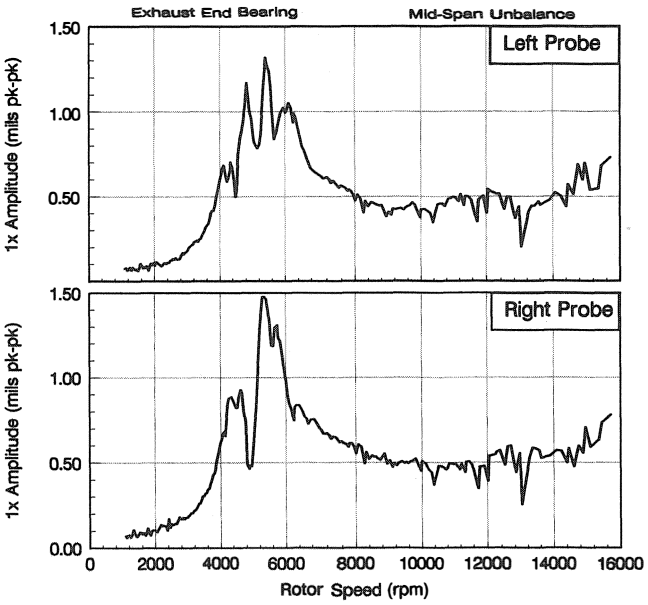

Figure 13. Measured Amplitude at Exhaust End Probes–Leading Edge Groove Bearing.

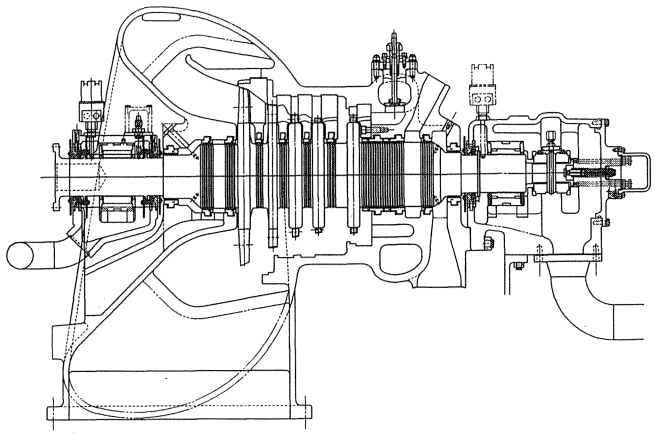

Figure 14. Layout of a Typical High Speed, Multistage Steam Turbine.

speed to attain the required separation margin. At lower operating speeds, the midshaft diameter can be reduced to 6.5 in to allow operation between critically damped first and second peak response speeds.

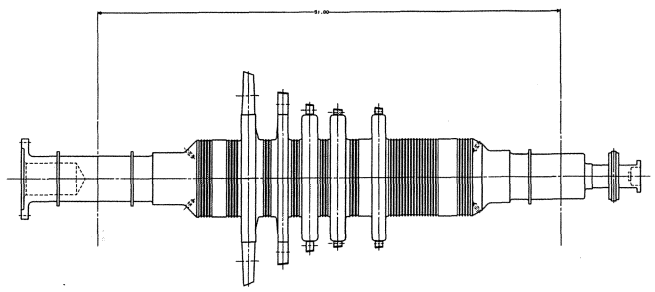

Figure 15. Schematic of a Five Stage Condensing Rotor.

To minimize the steam end overhang moment, speed pickup teeth were machined on the outside diameter of the thrust collar to eliminate a toothed wheel. The thrust bearing was kept as small as possible by stepping down the shaft diameter outboard of the journal. A flanged face at the shaft end provides for axial displacement probes, with grounding brushes located near the axial centerline. The exhaust end overhang was minimized by tucking the bearing case under the diffuser portion of the exhaust, and making the coupling flange integral with the rotor. Two radial displacement probes were included just inboard of each journal bearing, 45 degrees either side of top dead center. Two trim balance planes were provided as standard, one located at each end of the central shaft section.

Bearing Design

As a consequence of the successful tests on the laboratory turbine, leading edge groove journal and thrust bearings were incorporated into this design. The journal bearings, illustrated in Figure 16, were five pad, 5.0 in diameter by 3.75 in long, load between pivot. The design diametral bearing clearance and pad preload were nominally 9.25 mil and 0.33, respectively. These parameters were determined from a theoretical study on the influence of bearing geometry on rotor response. Oversize drain slots were machined into the bottom of the housing to allow spent hot oil to freely exit without partially flooding the bearing. The thrust bearing, shown in Figure 17, was of the self equalizing type with six pads of 12.5 in^2 total area per side.

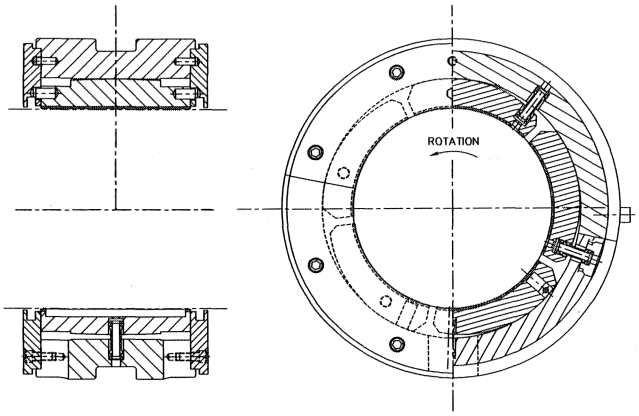

Figure 16. Leading Edge Groove Tilting Pad Journal Bearing.

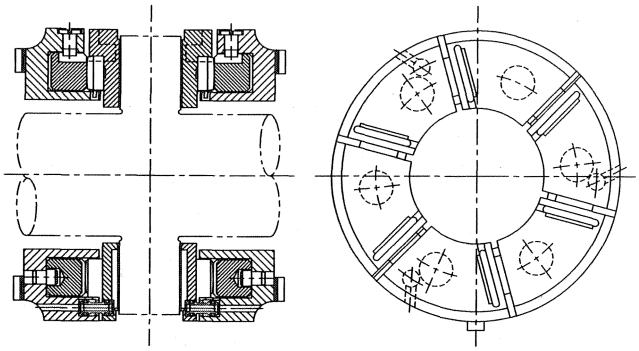

Figure 17. Leading Edge Groove Tilting Pad Thrust Bearing.

Although the primary purpose for using these bearings was to reduce operating pad temperature, reduced oil flowrates and frictional losses also were a requirement. The latter two can contribute to a reduced overall size of lubrication system, with associated cost savings.

FIRST PRODUCTION APPLICATION

The first production application employing leading edge groove bearings was a three stage backpressure turbine with a rated power of 2568 hp. The design operating range was from a minimum governor speed of 6826 rpm up to a maximum continuous speed of 14335 rpm. The bearings were designed for a 15 psig supply pressure and 120°F inlet temperature. The oil flowrate through each journal bearing was approximately 7.5 gpm, and the lubricant a light turbine oil.

The mass elastic model generated for the rotordynamics analysis is shown in Figure 18, and the undamped critical speed map in Figure 19. Included on the critical speed map are the resultant dynamic stiffness curves at nominal bearing clearances. These curves are derived from a series combination of the bearing and support characteristics as outlined by Nicholas, et al. [11]. The total rotor weight was 577 lb, yielding projected pad loads of 15.9 psi at the exhaust end and 14.8 psi at the steam end. Values of 3.0 $\times$ 10^6 lb/in and 150 lb were used for the support stiffness and mass at each bearing.

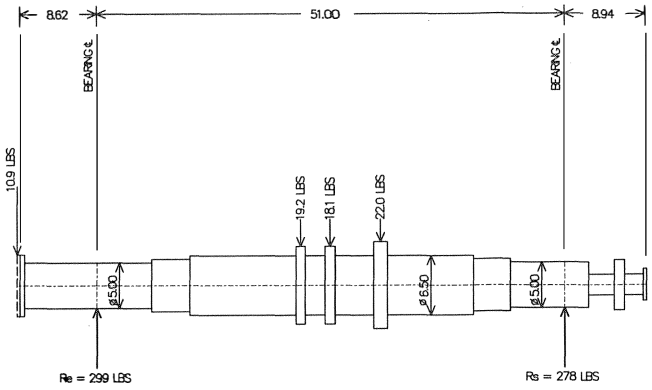

Figure 18. Mass Elastic Model of Rotor–First Production Application.

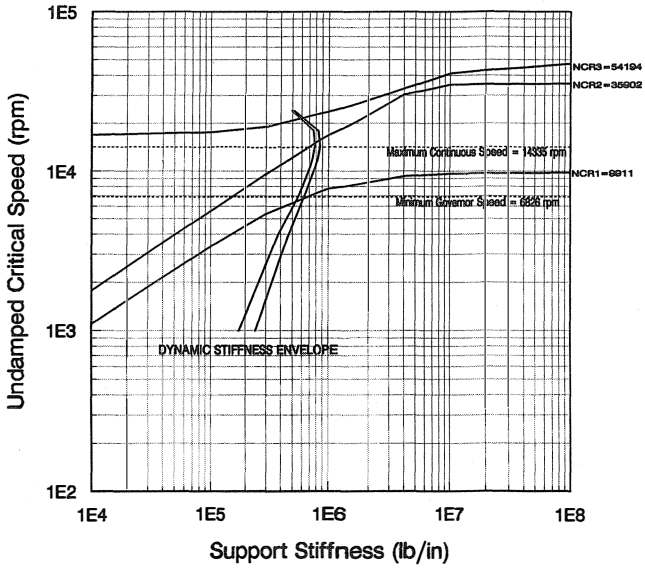

Figure 19. Undamped Critical Speed Map–First Production Application.

Stability

The results of an eigenvalue stability analysis at nominal bearing clearances are shown in Figure 20. The results are for the first forward whirl mode and associated logarithmic decrement. Values given are over a speed range up to 18000 rpm in increments of 3000 rpm. Included on the figure is the synchronous response line which intersects the first forward whirl speed curve at approximately 7700 rpm. The region of this intersection gives the general location of the first forward damped natural frequency. The values calculated for logarithmic decrement indicate theoretically that the rotor-bearing system is stable well beyond the maximum operating speed of 14335 rpm.

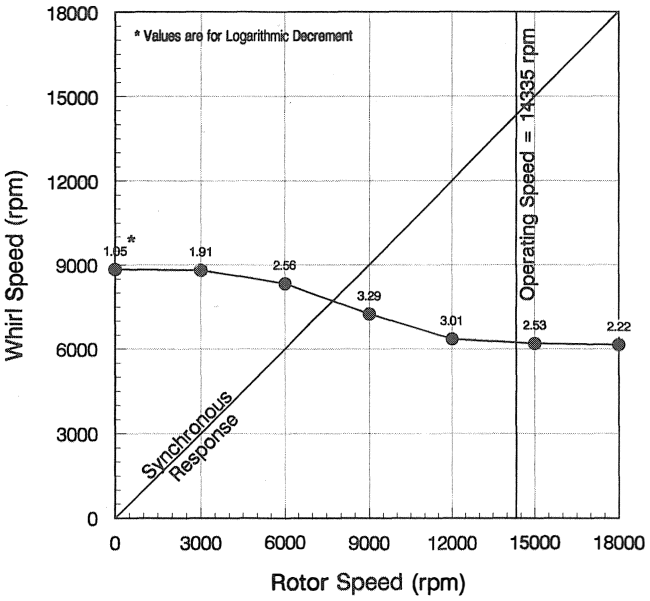

Figure 20. Whirl Speed and Logarithmic Decrement Vs *Speed–First Production Application.*

Unbalance Response

The predicted and measured synchronous amplitude and phase lag *vs* speed plots due to a first mode unbalance excitation are compared in Figures 21, 22, 23, and 24 at each probe location. This mode was excited by placing two weights in-phase at the trim balance planes. The magnitude of each weight was equivalent to an unbalance of eight times 4W/N, where W is the journal static load nearest each trim balance plane and N is the maximum continuous operating speed. Values for the location of the peak response speed, and associated amplification factor and maximum amplitude, are compared in Table 4.

Table 4. Comparison of Predicted and Measured Peak Response Speed (NC_1), Amplification Factor (AF_1), and Maximum Amplitude (A_{MAX})–First Production Application.

	SE LEFT			SE RIGHT			EE LEFT			EE RIGHT		
	NC_1 rpm	AF_1	A_{MAX} mils	NC_1 rpm	AF_1	A_{MAX} mils	NC_1 rpm	AF_1	A_{MAX} mils	NC_1 rpm	AF_1	A_{MAX} mils
PREDICTED	8275	1.5	0.35	8425	1.5	0.35	8200	1.6	0.39	8350	1.6	0.38
MEASURED	8053	4.4	0.39	8299	3.2	0.35	8053	4.2	0.29	7820	3.4	0.32

Overall, the correlation between the predicted and measured response is reasonable. The location of the peak response speeds are in good agreement to within a few hundred rpm. The measured peak response amplitudes deviate by less than 25 percent from those predicted, with the amplitude at the normal operating speed (13302 rpm) lower in every case. However, amplification factors were higher than predicted by almost a factor of three, and did not indicate a critically damped response. Nevertheless, even though the peak response was in the operating speed range, this test was accepted due to the low overall vibration levels.

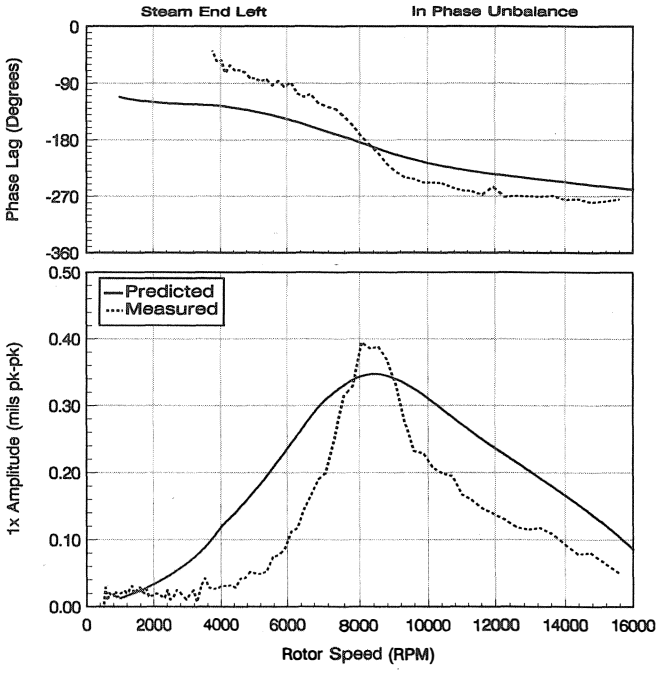

Figure 21. Comparison of Predicted and Measured Amplitude and Phase Lag at Steam End Left Probe–First Production Application.

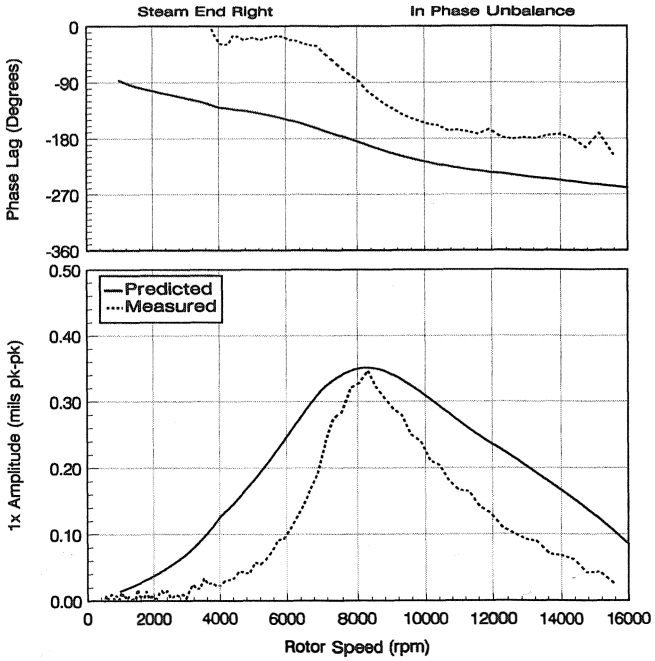

Figure 22. Comparison of Predicted and Measured Amplitude and Phase Lag at Steam End Right Probe–First Production Application.

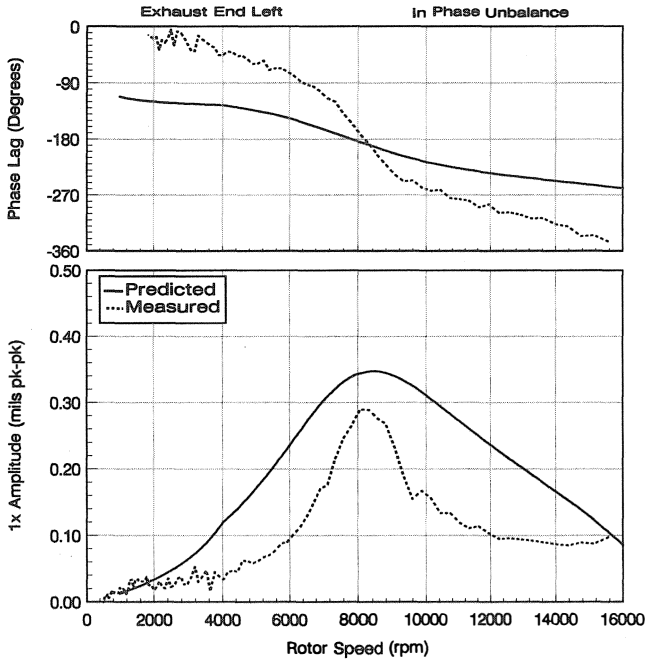

Figure 23. Comparison of Predicted and Measured Amplitude and Phase Lag at Exhaust End Left Probe–First Production Application.

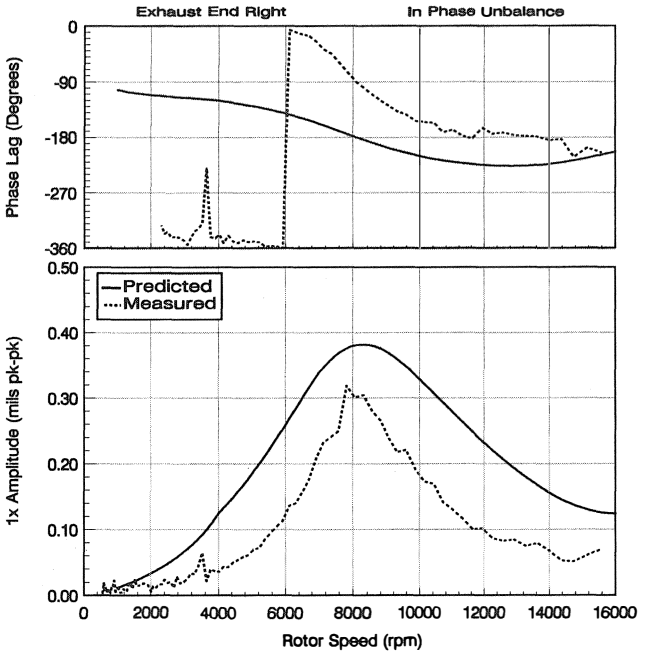

Figure 24. Comparison of Predicted and Measured Amplitude and Phase Lag at Exhaust End Right Probe–First Production Application.

SECOND PRODUCTION APPLICATION

The second production application also was a three stage backpressure machine with a rated power of 5037 hp. The design operating range was from a minimum governor speed of 9785 rpm up to a maximum continuous speed of 12843 rpm. However, for this application, steady state bearing performance was optimized by reducing the supply pressure to 7.5 psig. This reduced the oil flowrate through each journal bearing to 4.8 gpm. The oil inlet temperature was 120°F, and the lubricant a light turbine oil.

On this rotor, a taper hydraulic fit coupling was specified in preference to the integral coupling flange. The mass elastic model generated for the rotordynamics analysis is shown in Figure 25. The total rotor weight was 643 lb, giving specific pad loads of 18.0 psi at the exhaust end and 16.3 psi at the steam end. A value of 3.0×10^6 lb/in was used for the support stiffness, and 150 lb for the support mass.

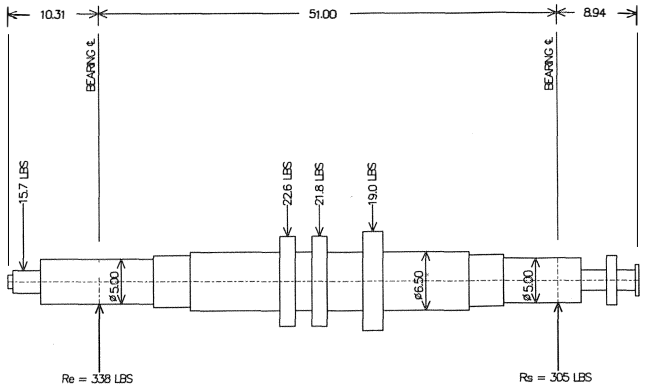

Figure 25. Mass Elastic Model of Rotor–Second Production Application.

Stability

The results of an eigenvalue stability analysis at nominal bearing clearances are shown in Figure 26. The results are for the first forward whirl mode and associated logarithmic decrement. Intersection with the synchronous response line gives an approximate value for the first forward damped natural frequency of 6500 rpm. Values for logarithmic decrement indicate theoretically that the rotor-bearing system is stable well beyond the maximum operating speed of 12843 rpm.

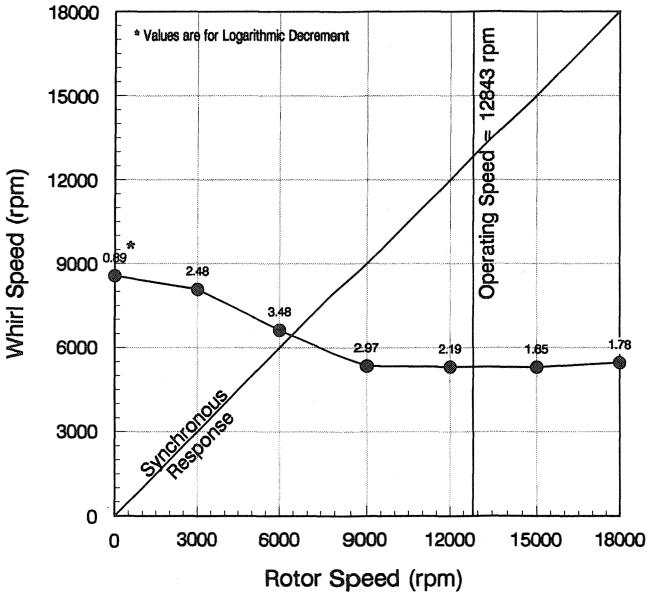

Figure 26. Whirl Speed and Logarithmic Decrement Vs Speed–Second Production Application.

During overspeed testing on this unit, however, the rotor-bearing system first went unstable at around 14000 rpm. With time and repeated attempts to run above the maximum continuous operating speed, the speed at which the system went unstable decreased. The frequency of this instability coincided approximately with the rotor's first lateral natural frequency of 8000 cpm (as revealed from the unbalance test). A typical spectrum plot at the steam end left probe is shown in Figure 27 at the maximum continuous operating speed of 12843 rpm. This figure shows a synchronous amplitude of less than 0.2 mil pk-pk with a subsynchronous component of nearly 1.4 mil pk-pk. When the machine went unstable, the subsynchronous component developed instantaneously and appeared as a pure spike. Higher subsynchronous amplitudes were reached with prolonged running.

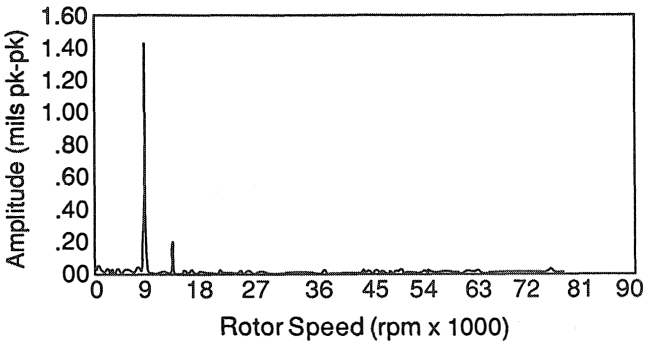

Figure 27. Frequency Spectrum at 12843 rpm with Original Groove Geometry: Steam End Left Probe–Second Production Application.

Although the precise mechanism initiating this instability was not conclusively determined, it is believed that the combination of high journal surface speed (>300 ft/sec) and extremely light pad load (<25 psi) are the contributing factors. Under these conditions, the journal is highly centered in the bearing and the pad attitude angle very small. Consequently, it could be possible that a divergent region exists near the trailing edge of the statically loaded pads, resulting in a film pressure profile with center that does not pass directly through the pivot. It is hypothesized that this condition could impose a moment on the pad that causes it to pitch resulting in a self excited unstable condition.

Since the pads were designed with a positive preload, pad flutter of the upper half (statically unloaded) pads was eliminated as a possible cause of this instability. Classical pad flutter occurs on upper pads when they become unloaded due to loss of hydrodynamic load. This condition arises when there does not exist a tilt angle at which the pads can seek an equilibrium position. However, in this application, the pads were designed with a preload of 0.33, which would require a bearing eccentricity ratio of greater than 0.49 in order for the upper most pad to lose its capacity to generate a hydrodynamic load (Equation (15), Nicholas [6]). In fact, due to the small pad loads involved, the bearing eccentricity ratio actually was predicted to be quite small (<0.15 at 12843 rpm), thus ensuring some hydrodynamic load generation on the upper pads. This small operating eccentricity ratio was confirmed by measurement of journal position from change in DC gap voltage at the radial displacement probes. Pad flutter was first analytically addressed by Adams and Payandeh [12] in a parametric study of statically unloaded pad vibration.

After some investigation, it was found that this instability could be eliminated by increasing the lubricant supply pressure. At 15 psig, the rotor ran smoothly at speeds well beyond 14000 rpm with no detectable sign of the subsynchronous vibration. The limiting pressure appeared to be in the range of 11 to 12 psig. However, 15 psig was chosen since this was the supply pressure used on the first unit which ran successfully and at a higher speed.

On this unit, however, increasing the supply pressure was not a viable option since additional oil flowrate was not available from the lubrication system. Consequently, a geometry modification to the leading edge groove was tried to stabilize performance. This modification is illustrated in Figure 28. It consisted of machining a taper on the exit side of the groove of each pad. The intent of this taper was to provide an additional force at the pad leading edge to increase the operating pad attitude angle. It is not known whether this force is due to the development of a hydrodynamic oil film wedge or to increased hydrostatic pressure in the tapered area adjacent to the groove. Nevertheless, this modification proved highly successful with trouble free operation up to a maximum speed of 15500 rpm (journal surface speed of 338 ft/sec) at the design supply pressure of 7.5 psig. Design constraints of the blading prohibited operation at higher speeds on this unit. An equivalent spectrum plot at the steam end left probe for an operating speed of 12843 rpm is shown in Figure 29. Clearly, there is no sign of the subsynchronous vibration (or instability) previously encountered, with the synchronous amplitude again less than 0.2 mil pk-pk. (Note, in Figures 27 and 29, the scales have been kept the same for comparison.)

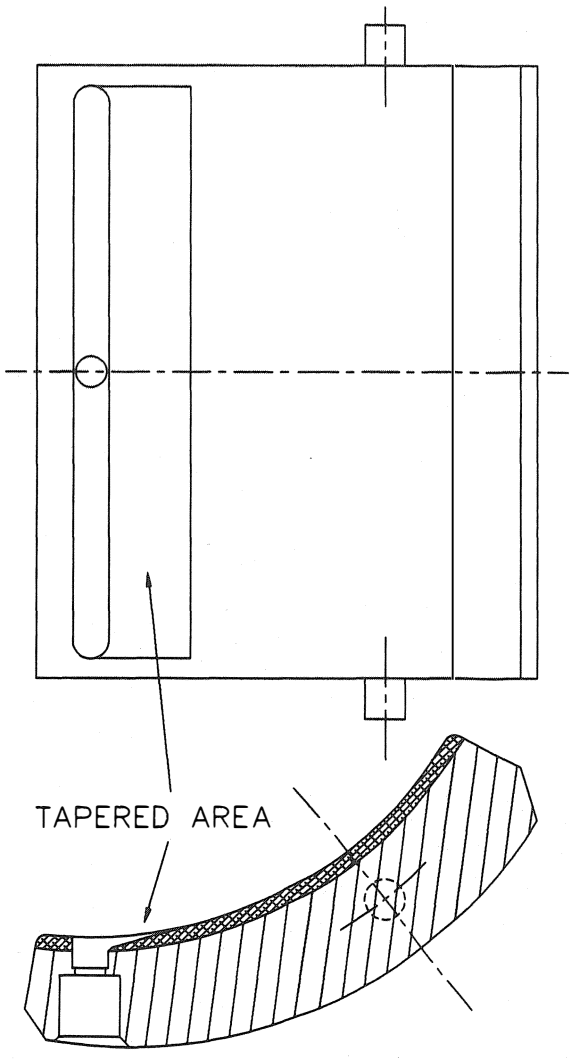

Figure 28. Sectional View Illustrating Tapered Modification to Leading Edge Groove.

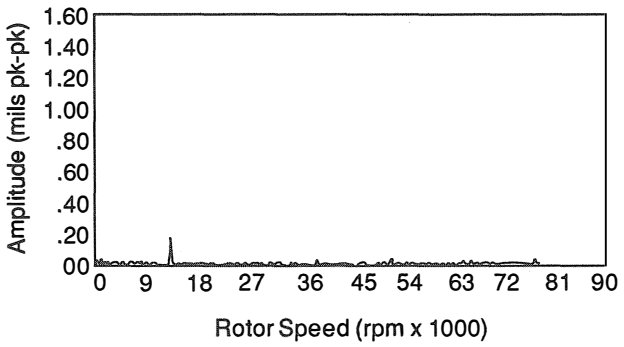

Figure 29. Frequency Spectrum at 12843 rpm with Tapered Groove Geometry: Steam End Left Probe–Second Production Application.

Unbalance Response

During unbalance testing with the tapered groove bearing at 7.5 psig supply pressure, it was observed that the amplitude and amplification factor on passing through the first peak response speed were reduced. Unbalance response data comparing the original bearing at 15 psig with the tapered groove design at 7.5 psig are given in Figures 30, 31, 32, and 33. Included on the figures is the predicted response from the original rotordynamics analysis. These results are summarized in Table 5 that compares the location, amplification factor, and maximum amplitude of the predicted peak response speed with the measured values. This mode was excited by placing two weights in-phase at the trim balance planes, of magnitude equivalent to an unbalance of eight times 4W/N.

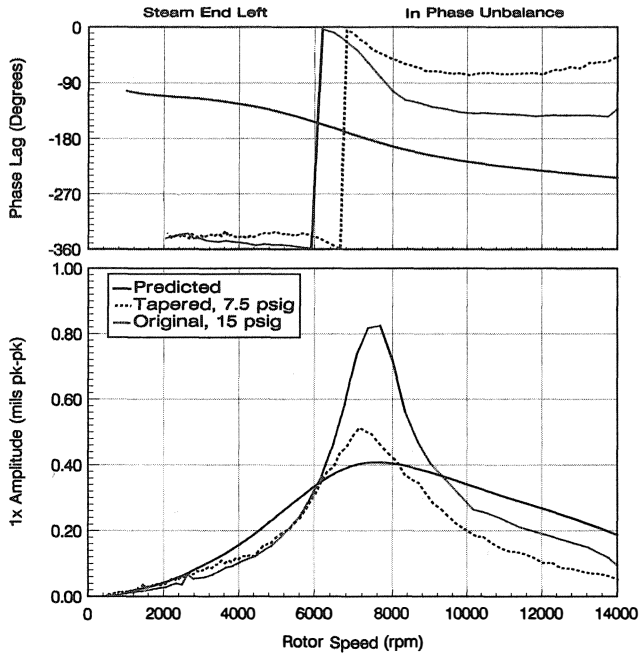

Figure 30. Comparison of Predicted and Measured Amplitude and Phase Lag at Steam End Left Probe: Original and Tapered Groove Geometries–Second Production Application.

The tapered groove clearly has a significant improvement on rotor response over the original design. This is particularly evident at the first peak response speed, with the maximum amplitude lower at all four probes by almost a factor of two. Vibration amplitudes at running speed also are lower, by approximately one half. Nevertheless, although amplification factors are noticeably lower at the left side probes, they are slightly higher at the right.

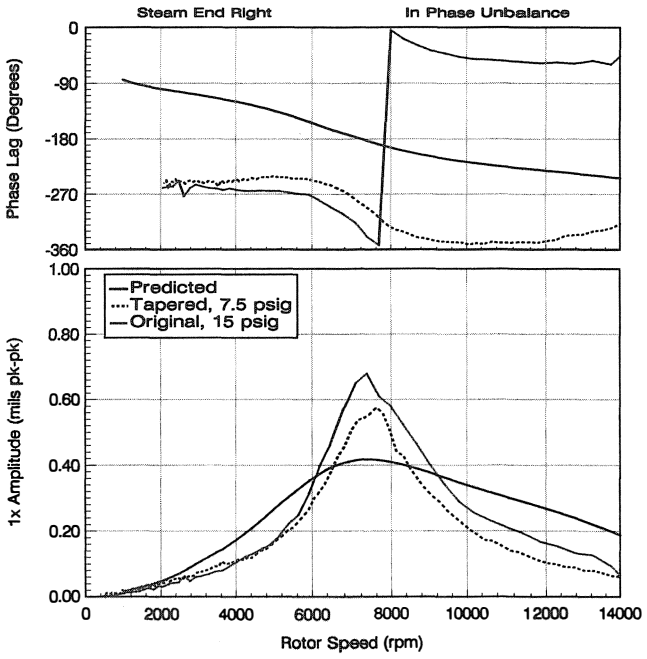

Figure 31. Comparison of Predicted and Measured Amplitude and Phase Lag at Steam End Right Probe: Original and Tapered Groove Geometries–Second Production Application.

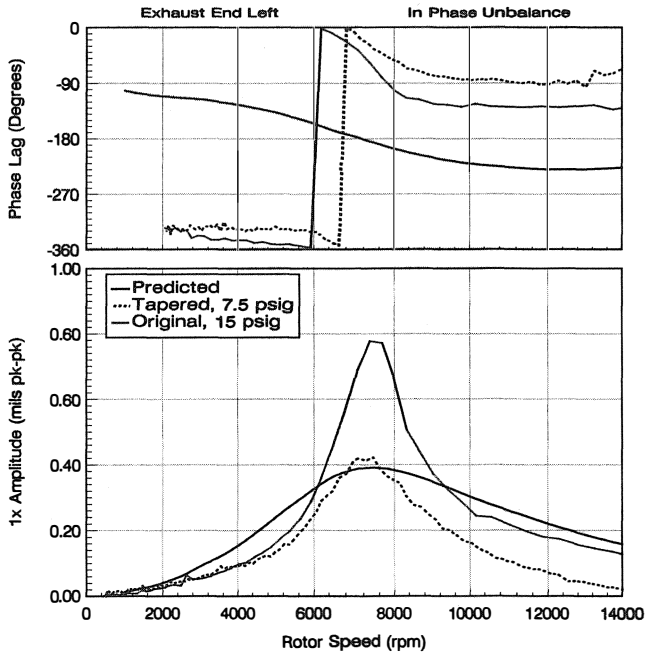

Figure 32. Comparison of Predicted and Measured Amplitude and Phase Lag at Exhaust End Left Probe: Original and Tapered Groove Geometries–Second Production Application.

It is noteworthy that with the original bearing design, the observed trend with amplification factor being higher at the left probes is consistent with the results on the first application. With the tapered groove design, this trend is reversed with the higher amplification factors occurring at the probes located on the right.

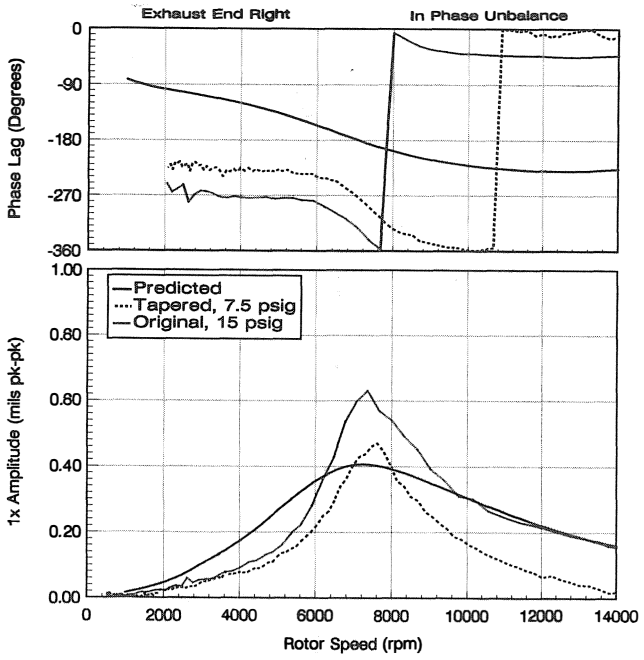

Figure 33. Comparison of Predicted and Measured Amplitude and Phase Lag at Exhaust End Right Probe: Original and Tapered Groove Geometries–Second Production Application.

Table 5. Comparison of Predicted and Measured Peak Response Speed (NC_1), Amplification Factor (AF_1), and Maximum Amplitude (A_{MAX}): Original and Tapered Leading Edge Groove Geometries–Second Production Application.

	SE LEFT			SE RIGHT			EE LEFT			EE RIGHT		
	NC_1 rpm	AF_1	A_{MAX} mils	NC_1 rpm	AF_1	A_{MAX} mils	NC_1 rpm	AF_1	A_{MAX} mils	NC_1 rpm	AF_1	A_{MAX} mils
PREDICTED	7400	1.4	0.42	7600	1.5	0.41	7200	1.4	0.41	7400	1.4	0.39
ORIGINAL w/15.0 psig	7678	5	0.83	7355	3.5	0.68	7355	4.9	0.78	7355	3.3	0.63
TAPERED w/7.5 psig	7123	3.1	0.51	7623	3.8	0.58	7455	3.4	0.42	7623	3.9	0.47

Accuracy of Theoretical Model

The theoretical model unquestionably is deficient. The unbalance response analysis clearly shows that the effective system damping on passing through the first peak response speed is over-predicted as measured by amplification factor. This also is reflected in the stability analysis which indicates a highly stable system. This discrepancy most likely arises from the bearing model in the calculation of the stiffness and damping coefficients at these light loads. Work is planned to improve understanding and correlation of the bearing theory with actual performance. To some extent, this trend regarding amplification factor also has been observed with flooded bearings.

THIRD PRODUCTION APPLICATION

The third production application was a four stage backpressure unit with a rated power of 4349 hp. The design operating range was from a minimum governor speed of 5736 rpm up to a maximum continuous speed of 8772 rpm. Since, on this application, the calculated first peak response speed was in the operating range, four bearing configurations were evaluated to determine the optimum combination of groove geometry and supply pressure to ensure a critically damped peak response speed (as defined in API 612 [1]). The oil inlet temperature was 120°F, and the lubricant a light turbine oil.

The mass elastic model generated for the rotordynamics analysis is shown in Figure 34. The total rotor weight was 773 lb, resulting in projected pad loads of 21.9 psi at the exhaust end and 19.4 psi at the steam end. Values of 3.0×10^6 lb/in and 150 lb were again used for the support stiffness and mass. A central trim balance plane was included on this rotor in addition to those located inboard of the journal bearings.

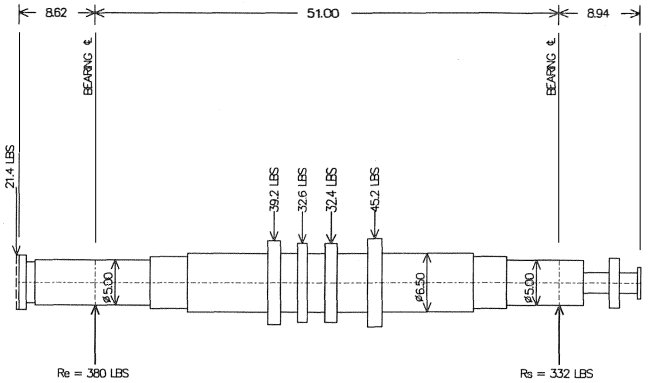

Figure 34. Mass Elastic Model of Rotor–Third Production Application.

Description of Groove Geometries and Test Conditions

Cross sectional views depicting the three leading edge groove geometries tested are illustrated in Figure 35. The tapered and pocket geometries were machined across the entire axial length of the feed groove, and were added to all five pads. All three geometries were tested with a lubricant supply pressure of 7.5 psig. A fourth test was conducted on the original design with the supply pressure increased to 20 psig.

Unbalance Response

All tests were conducted with a first mode unbalance excitation by placing a weight at the rotor's central trim balance plane. The magnitude of this weight was equivalent to an unbalance of four times 4W/N. Coast down data of the measured amplitude and phase lag for this unbalance condition are given in Figures 36, 37, 38, and 39. For comparison, the measured response from all four tests are included on the same plot. Values for the location of the peak response speed, amplification factor, and maximum amplitude are compared in Table 6.

Table 6. Comparison of Measured Peak Response Speed (NC_1), Amplification Factor (AF_1), and Maximum Amplitude (A_{MAX}): Original, Tapered, and Pocket Leading Edge Groove Geometries–Third Production Application.

	SE LEFT			SE RIGHT			EE LEFT			EE RIGHT		
	NC_1 rpm	AF_1	A_{MAX} mils	NC_1 rpm	AF_1	A_{MAX} mils	NC_1 rpm	AF_1	A_{MAX} mils	NC_1 rpm	AF_1	A_{MAX} mils
ORIGINAL w/7.5 psig	7102	3.8	0.59	7102	10.2	1.18	7672	3.6	0.55	7102	9.8	0.92
ORIGINAL w/20.0 psig	7020	4	0.82	7020	3.4	0.71	7410	4.1	0.78	7020	2.6	0.64
TAPERED w/7.5 psig	6959	3	0.6	7073	3.6	0.61	7419	2.6	0.61	7073	2.3	0.55
POCKET w/7.5 psig	6699	2.6	0.59	7008	2.7	0.62	6551	2.1	0.62	7008	2.2	0.58

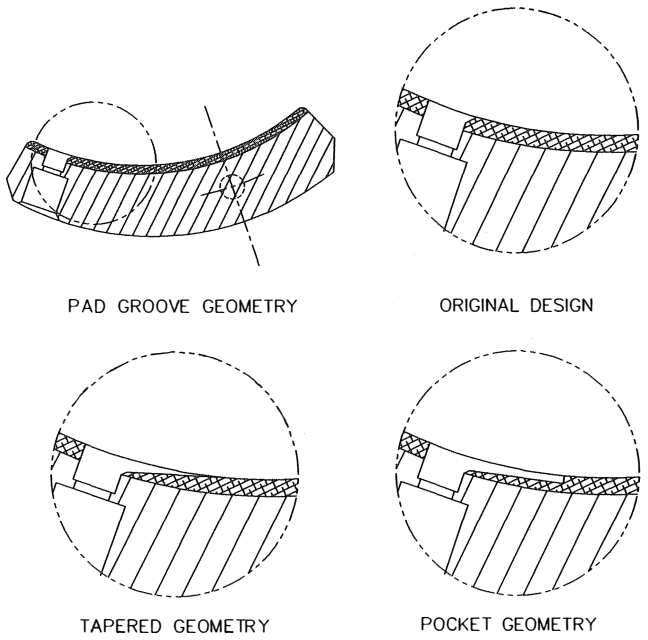

Figure 35. Sectional Views Illustrating the Leading Edge Groove Geometries of the Original, Tapered, and Pocket Designs.

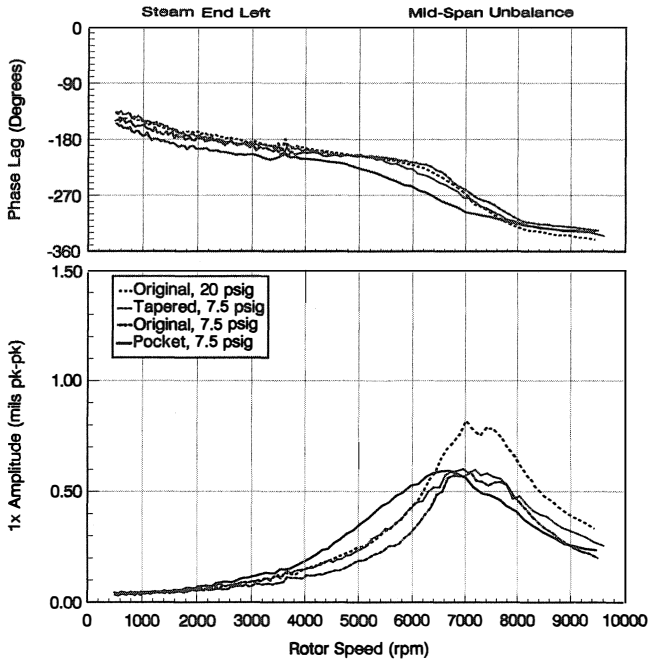

Figure 36. Comparison of Measured Amplitude and Phase Lag at Steam End Left Probe–Third Production Application.

With the original groove design, increasing the supply pressure from 7.5 to 20 psig significantly improved the overall response, particularly as observed at the probes on the right located near the orbit major axis. However, at the left probes, both amplitude and amplification factor were slightly increased and higher than at the right probes. This is consistent with observations on the second application. The downside to this, however, is that the oil flowrate through the bearing is increased, which infringes on one of the

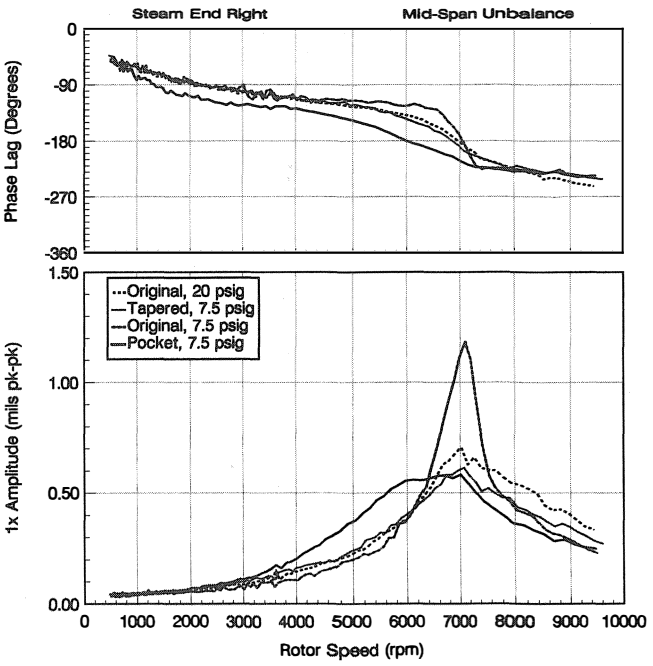

Figure 37. Comparison of Measured Amplitude and Phase Lag at Steam End Right Probe–Third Production Application.

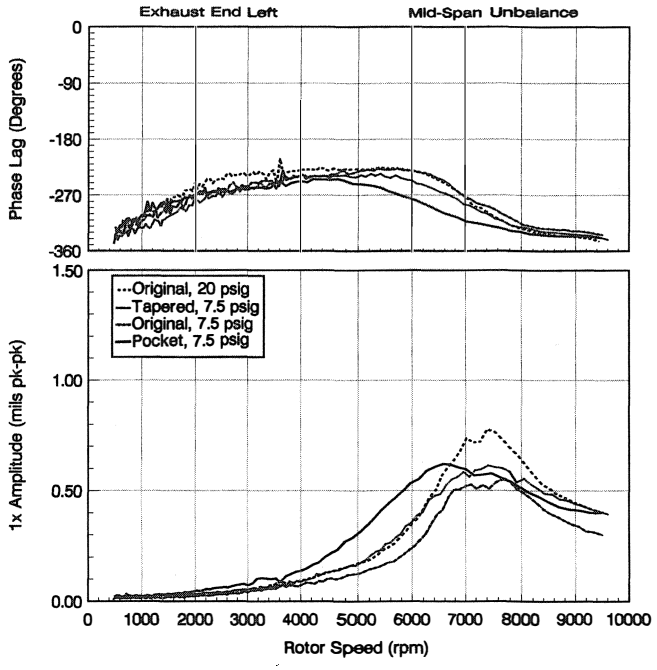

Figure 38. Comparison of Measured Amplitude and Phase Lag at Exhaust End Left Probe–Third Production Application.

primary reasons for using this design (reduced flow, power loss, and lubrication system size.)

Of greater interest, however, is that both the tapered and pocket geometries at 7.5 psig supply pressure yielded further improvements in overall response. Both geometries resulted in additional reductions in both amplitude and amplification factor, with the pocket geometry the slightly better of the two. Furthermore, the

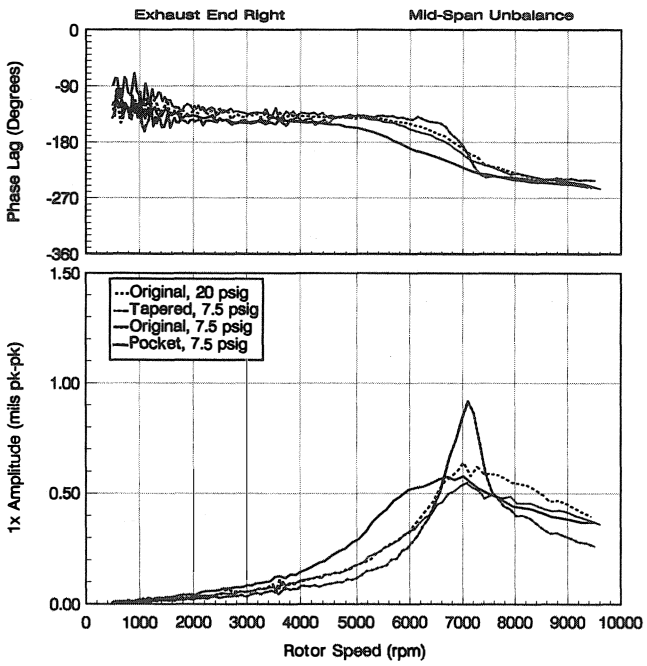

Figure 39. Comparison of Measured Amplitude and Phase Lag at Exhaust End Right Probe–Third Production Application.

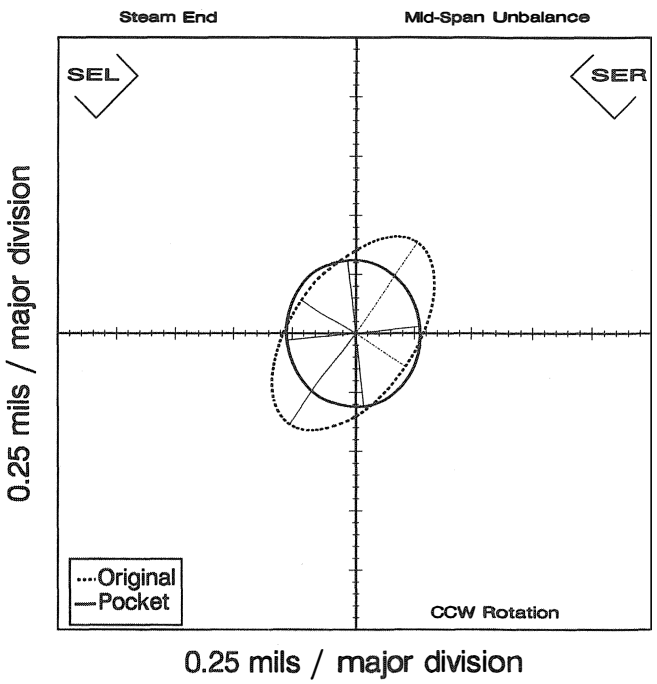

Figure 40. Measured Synchronous Filtered Orbit at Steam End Peak Response Speed: Original and Pocket Groove Geometries–Third Production Application.

pocket geometry also yielded a slight reduction in the general location of the peak response speed. With regard to amplification factor, the trend generally agrees with the observations on the second application with the tapered geometry, in that the higher values occurred at the right probes.

Synchronous filtered orbits derived from the steam and exhaust end probes are given in Figures 40 and 41 at the first peak response speed. The orbits shown compare the original design with what is considered to be the most optimum modification tested, the pocket geometry. The data presented are both for a supply pressure of 7.5 psig. Of particular interest is the change in orbit shape from one that is highly elliptical with the original design, to one that is almost circular with the pocket geometry. In general, circular orbits are preferable since their vibration amplitudes are smaller on passing through peak response speeds compared to the major axis of an elliptical orbit.

Steady State Performance

Bearing steady state performance was not greatly affected. Temperature data at the exhaust end instrumented pads are compared in Table 7 over a speed range up to 9500 rpm. Design constraints of the blading limited testing at higher speeds. The temperature sensors were located at the 75 percent position from the pad leading edge. Unquestionably, the change in supply pressure and groove geometry had a minimal effect on the measured value of pad temperature, with the variation less than 10°F. Furthermore, on all configurations tested, the measured temperatures at both instrumented pads were nearly equal, with the maximum difference less than 5.0°F.

A quantitative comparison of power loss was not possible. This was because oil drain temperatures were measured by a thermometer placed in the drain line. Although the position of this thermometer was not changed during the testing, it likely was not in the optimum temperature location. Nevertheless, the indicated readings were very consistent with the maximum variation in temperature of less than 4.0°F between all three designs tested at 7.5 psig supply pressure. Consequently, it can be reasonably concluded that the geometry modifications have little effect on power loss.

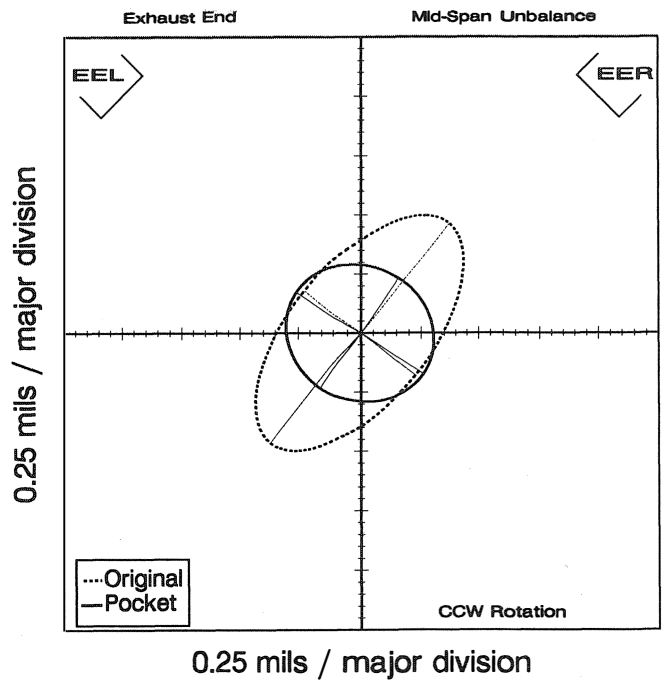

Figure 41. Measured Synchronous Filtered Orbit at Exhaust End Peak Response Speed: Original and Pocket Groove Geometries–Third Production Application.

Table 7. Comparison of Exhaust End Pad Metal Temperature: Original, Tapered, and Pocket Leading Edge Groove Geometries–Third Production Application.

SPEED	ORIGINAL			ORIGINAL			TAPERED			POCKET		
(rpm)	w/7.5 psig			w/20.0 psig			w/7.5 psig			w/7.5 psig		
	OIL FLOW gpm	EE LEFT °F	EE RIGHT °F	OIL FLOW gpm	EE LEFT °F	EE RIGHT °F	OIL FLOW gpm	EE LEFT °F	EE RIGHT °F	OIL FLOW gpm	EE LEFT °F	EE RIGHT °F
1000	4.5	125	125	7.0	124	124	4.5	128	128	4.5	125	126
2000	4.5	130	130	7.9	127	127	4.5	133	133	4.3	131	132
3000	4.7	134	133	8.0	134	132	4.5	136	136	4.2	134	135
4000	4.8	136	134	8.0	137	135	4.5	139	138	4.5	137	138
5000	4.9	138	137	9.0	140	138	4.9	141	139	4.6	139	141
6000	4.9	143	141	9.0	142	140	4.9	144	143	4.7	141	142
7000	4.9	146	144	9.0	148	144	4.9	152	149	4.9	147	148
8000	4.9	151	150	9.0	150	146	4.9	151	147	4.9	149	149
9000	4.8	156	154	9.0	154	149	4.9	153	149	4.8	154	155
9500	4.8	157	156	9.0	155	150	4.9	160	155	4.9	157	158

CONCLUSIONS

The primary conclusion that can be drawn from this work is that current rotor-bearing analysis techniques are not flawless. The case histories discussed complied with all generally accepted rotordynamics criteria, and yet, when tested, exhibited an instability and higher than predicted vibration on passing through the first lateral natural frequency. The main source of error most likely was the bearing model at the light pad loads of these applications. Clearly, much remains to be learned about the dynamic performance of tilting pad journal bearings at these immoderate conditions. Work is planned that will improve both understanding and correlation of the theory with actual performance.

Specific conclusions from this investigation are summarized as follows:

• An experimental evaluation of a leading edge groove tilting pad journal bearing showed a significant reduction in pad temperature compared with a conventional flooded design. With the leading edge groove bearing, both loaded pads operated at about the same maximum pad temperature unlike a flooded bearing in which there can be a significant temperature difference between pads.

• With the leading edge groove bearing, lower pad temperatures were achieved with approximately 50 percent less oil flowrate than used for the flooded bearing. The leading edge groove bearing also reduced power loss, with the largest difference occurring at the highest speed tested. At 16000 rpm, a reduction in power consumed of approximately 25 percent was observed.

• In a production application employing leading edge groove bearings, rotor-bearing dynamic performance was found to noticeably deviate from that predicted by theory. This discrepancy most likely originated from the bearing model at these immoderate loads (<25 psi), where the applicable limits of established tilting pad journal bearing theory are stretched.

• Adding a tapered or pocket geometry to the exit side of the leading edge groove greatly improved the bearing's dynamic performance at these light loads. The pocket geometry yielded the best overall improvement.

• The tapered and pocket geometries are believed to generate a supplemental pressure force at the pad leading edge. The result is a change in the bearing's dynamic characteristics that yields improved vibration suppression from the oil film. The observed benefit was in terms of both lower vibration amplitudes and improved rotor-bearing stability.

• With the pocket geometry, the highest amplification factor on passing through the first peak response speed was reduced by a factor of greater than four compared with the original design at the same supply pressure. The vibration amplitude at the design operating speed also was reduced, by a factor of almost two.

• Increasing the supply pressure or modifying the groove geometry (with either the tapered or pocket design) had little effect on temperature rise across the oil film as observed at the instrumented location.

• This modification was proven on very lightly loaded tilting pad journal bearings with projected loads of less than 25 psi. There likely is an upper limit of bearing load beyond which this supplemental leading edge pressure force has negligible or no influence on dynamic performance. This was not investigated.

NOMENCLATURE

A_{MAX} = maximum vibration amplitude at NC_1 (mil)
AF_1 = amplification factor at NC_1 (dim)
D = journal diameter (in)
L = bearing axial length (in)
N = maximum continuous operating speed (rpm)
NC_1 = first peak response speed (rpm)
Re = exhaust end journal load (lbf)
Rs = steam end journal load (lbf)
W = rotor weight (lbf)

REFERENCES

1. American Petroleum Institute Standard 612, "Special-Purpose Steam Turbines for Refinery Services," American Petroleum Institute, Washington D. C., Fourth Edition (1995).
2. Mikula, A. and Gregory, R., "A Comparison of Thrust Bearing Lubricant Supply Methods," ASME Journal of Lubrication Technology, *105,* pp. 39-47 (1981).
3. Tanaka, M., "Thermohydrodynamic Performance of a Tilting Pad Journal Bearing With Spot Lubrication," ASME Journal of Tribology, *113,* pp. 615-619 (1991).
4. Harangozo, A. V., Stolarski, T. A., and Gozdawa, R. J., "The Effect of Different Lubrication Methods on the Performance of a Tilting Pad Journal Bearing," STLE Tribology Transactions, *34,* pp. 529-536 (1991).
5. Dmochowski, W., Brockwell, K., DeCamillo, S., and Mikula, A., "A Study of the Thermal Characteristics of the Leading Edge Groove and Conventional Tilting Pad Journal Bearings," ASME Journal of Tribology, *115,* pp. 219-226 (1993).
6. Nicholas, J. C., "Tilting Pad Bearing Design," *Proceedings of the Twenty-Third Turbomachinery Symposium,* The Turbomachinery Laboratory, Texas A&M University, College Station, Texas (1994).
7. Edney, S. L., "Pad Temperature in High Speed, Lightly Loaded Tilting Pad Journal Bearings," *Proceedings of the Twenty-Fourth Turbomachinery Symposium,* The Turbomachinery Laboratory, Texas A&M University, College Station, Texas (1995).
8. Brockwell, K., Dmochowski, W., and DeCamillo, S., "Analysis and Testing of the LEG Tilting Pad Journal Bearing - A New Design for Increasing Load Capacity, Reducing Operating Temperatures and Conserving Energy," *Proceedings of the Twenty-Third Turbomachinery Symposium,* The Turbomachinery Laboratory, Texas A&M University, College Station, Texas (1994).
9. American Petroleum Institute Standard 670, "Vibration, Axial-Position and Bearing Temperature Monitoring Systems,"

American Petroleum Institute, Washington D. C., Second Edition (1986).

10. Brockwell, K. R. and Kleinbub, D., "Measurements of the Steady State Operating Characteristics of the Five Shoe Tilting Pad Journal Bearing," STLE Tribology Transactions, *32,* pp. 267-275 (1989).
11. Nicholas, J. C., Whalen, J. K., and Franklin, S. D., "Improving Critical Speed Calculations Using Flexible Bearing Support FRF Compliance Data," *Proceedings of the Fifteenth Turbomachinery Symposium,* The Turbomachinery Laboratory, Texas A&M University, College Station, Texas (1986).
12. Adams, M. L. and Payandeh, S., "Self-Excited Vibration of Statically Unloaded Pads in Tilting-Pad Journal Bearings," ASME Journal of Lubrication Technology, *105,* pp. 377-384 (1983).

ACKNOWLEDGMENTS

The authors would like to thank Dresser-Rand Engineering Laboratory Staff for building and operating the test turbine, and Shop Floor Test Personnel for building and operating the production turbines. Thanks also are due to Kingsbury Repair and Service Division for their quick response in manufacturing the groove geometries tested. Finally, they would like to express their gratitude to the Directors of Dresser-Rand Steam Turbine Division and Kingsbury, Inc., for permission to publish the material contained herein.